

# Bessel-like Beam Array Generation Using Round-tip Microstructures and Their Use in the Material Treatment

Evaldas Stankevičius, Mantas Garliauskas and Gediminas Račiukaitis

Center for Physical Sciences and Technology, Savanoriu Ave. 231, LT-02300 Vilnius, Lithuania  
E-mail: estankevicius@ftmc.lt

Generation of Bessel-like beam array from polymeric microstructures, which were created using four-beam interference lithography is demonstrated. Quality of the produced Bessel-like beams depends on the geometrical parameters of the manufactured axicon-like structures, and their shape can be efficiently controlled through the laser treatment parameters. The output beam characteristics indicate the characteristic features of Bessel beams. The created Bessel-like beams were used for photopolymerisation, ablation and thin-film ink coated glass modification in order to show the material treatment abilities by the generated Bessel-like beams. The presented strategy of micro-optics formation could be employed not only for the material treatment but also for a simple creation of angular-tolerant wavefront detectors, optical imaging systems, optical tweezers, etc.

DOI: 10.2961/jlmn.2016.03.0013

**Keywords:** Bessel beam, interference lithography, micro-optics, polymeric structures, photopolymerisation;

## 1. Introduction

Bessel beams [1] because of their extraordinary properties (spread invariance and self-recreation [2,3]) are broadly utilized in numerous fields: optical lithography [4], cell transfection [5], optical manipulation [6,7], microscopy [8], optical pumping [9], laser ablation [10,11], nuclear transport [12] and catching [13,14], and more. The most known strategy for Bessel beam generation is the usage of axicons [15] because of their high efficiency in beam transformation. Microaxicons are exceptionally alluring components for Bessel beam applications in microscopic scale (e. g. catching of cells or nanoparticles) due to their integrability and low weight. There are different approaches to manufacturing microaxicons or axicon-like components: electric-field-induced self-organization [16], direct laser photopolymerization [17], electron beam lithography [18], vapour phase deposition of dielectric layers through shadow masks [19], reactive-ion etching [20], etc. In this work, we exhibit a simple, fast and flexible strategy to manufacture microaxicons via the four-beam interference lithography. Characteristics of the output beams show that the fabricated polymeric structures generate Bessel-like beams. An easy fabrication method of axicom matrix paves the way for the development of tilt-tolerant wavefront sensors, new optical imaging systems, novel materials treatment tools or optical tweezers.

## 2. Materials and Methods

Microaxicon-like structures were created using the four-beam interference lithography technique [21] (Fig. 1) from the hybrid organic-inorganic Zr-containing negative photoresist SZ2080 [22] (FORTH, Greece) enriched with the photoinitiator 4,4'-bis(dimethylamino)-benzophenone (concentration by weight equal to 0.5%).

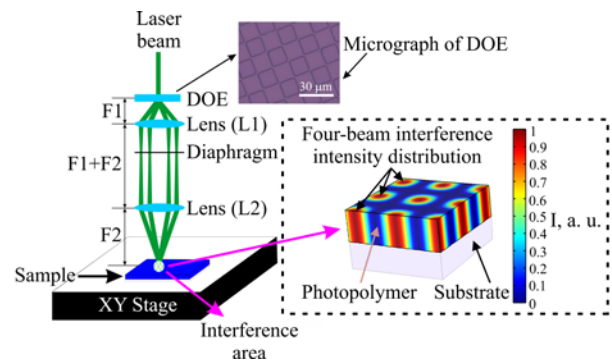


**Fig. 1** The four-beam interference lithography experimental setup.

In the manufacturing procedure, a Yb:KGW femtosecond laser (Pharos, Light Conversion) radiating pulses with a duration of 250 fs at a 100 kHz repetition rate and 515 nm wavelength of irradiation was employed. Four identical laser beams (1<sup>st</sup> order of diffraction maxima) were obtained by splitting the laser beam with a diffractive optical element (DOE) (Holo-Or Ltd.) with the 1.4 deg separation angle between beams. The undesirable diffraction maximums of zero and higher than the first orders (not shown in Fig. 1) were blocked by a diaphragm. The obtained four beams were collected by the two-lens imaging system (L1 with the focal length  $F_1=25$  mm and L2 with the focal length  $F_2=100$  mm) in order to generate a four-beam interference pattern (Fig. 1 (right)). The period of the obtained interference pattern can be adjusted by varying magnification of the two-lens imaging system [23]. The four-beam interference pattern with 60  $\mu\text{m}$  period was recorded into SZ2080 photopolymer sample, which was prepared by using a spin-coating method. Before the laser treatment, the samples were heated for  $\sim 20$  min at 95°C to evaporate the solvent and solidify the samples. The photopolymerisation process was initiated in a solid state of the

material. After the photomodification, samples were immersed into 4-methyl-2-pentanone for 20 min to dissolve unmodified polymer parts.

### 3. Results and Discussion

Two kinds of microstructure arrays have been manufactured using the four-beam interference lithography technique, which we call them type I, II (shown in Fig. 2). The particular research on the structures formation using the four-beam interference lithography was analysed in our paper [24]. The research results show that the geometry of the structures depends on the laser irradiation dose. The higher the laser irradiation dose, the taller and wider pillars can be fabricated (profiles in Fig. 2).

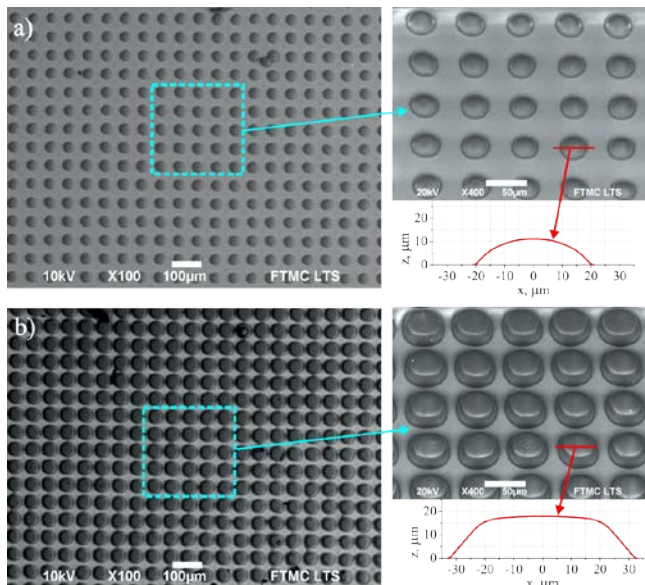


**Fig. 2** SEM micrographs at different magnification and profiles of structures produced via the four-beam interference lithography using a different laser irradiation dose: a)  $\sim 4.7$  J (the average laser power  $\sim 0.47$  W and laser exposure time 10 s); b)  $\sim 27.9$  J (the average laser power  $\sim 0.93$  W and laser exposure time 30 s). The period is  $\sim 60$   $\mu\text{m}$ . The structures in right SEM images are tilted by 34 deg.

Optical properties of the manufactured structures were examined by the optical performance test system (Fig. 3). This system contains a laser (wavelength 532 nm), a 3D positioning system, an objective and a CCD camera. The magnification of the system was 19. In order to characterise beams formed by the fabricated structures, a glass plate with the test structure was located before the objective at the distance larger than the focal length of the objective (11 mm). Propagation of the beam behind the sample was registered by moving the sample in the  $z$  direction.

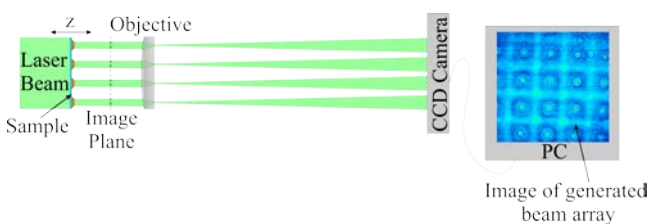


**Fig. 3** The scheme of the optical performance test system.

The results of optical properties test of two type structures are shown in Fig. 4. The results exhibit that both types of manufactured structures generate the beams with concentric rings. Despite that the intensity distributions of the generated beams are slightly varying with the axial position  $z$ , the intensity distribution with the series of concentric rings alludes to the Bessel beam intensity distribution that is proportional to the square of zero-order Bessel function of the first kind:

$$I(r, \beta) \propto J_0^2(k_{\perp} r) \quad (1)$$

where  $r$  is the radial coordinate;  $k_{\perp}$  is the perpendicular wave vector component which is related to the wavelength  $\lambda$  and the half apex angle  $\beta$  of the cone by

$$k_{\perp} = 2\pi \sin\beta / \lambda \quad (2)$$

The change of the spatial frequency of the generated beam fringe pattern means that the conical beam angle  $\beta$  is a function of the axial position  $z$  ( $\beta(z)$ ). [25]

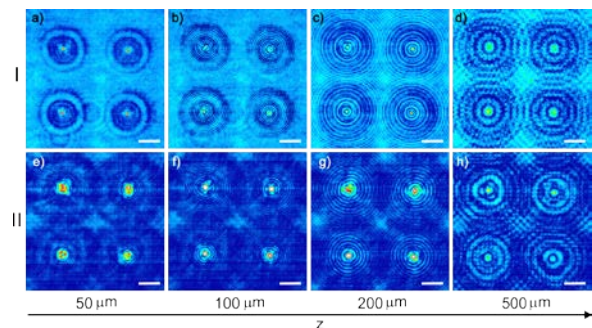


**Fig. 4** Beams intensity distributions exiting from the different type of the structures (type I (a,b,c,d), type II (e,f,g,h)) in the transverse plane, at different distances from the tip of the structures: 50  $\mu\text{m}$  (a,e); 100  $\mu\text{m}$  (b,f); 200  $\mu\text{m}$  (c,g); 500  $\mu\text{m}$  (d,h). The scale bars represent 20  $\mu\text{m}$ . [26]

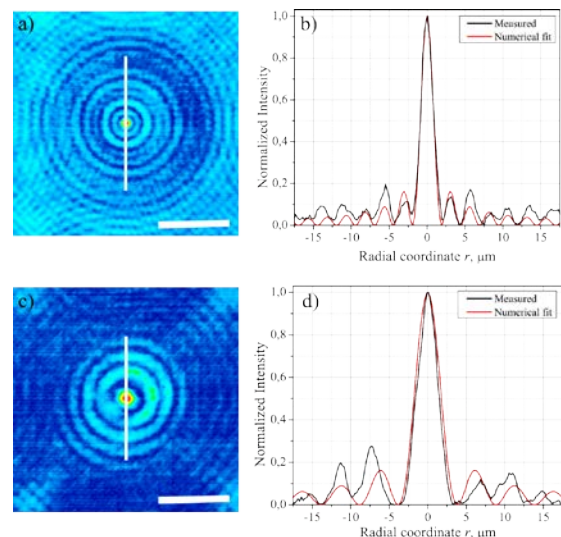


**Fig. 5** Intensity distributions of the generated beams formed using different types of the structures: a) I; c) II; at the distance of 200  $\mu\text{m}$  (a) and 350  $\mu\text{m}$  (c) from the sample and the comparison of the transverse intensity profiles taken along the white line (black curves) with the numerical fit of the Bessel beam intensity distribution when  $k_{\perp}=1.15$  (b) and  $k_{\perp}=0.65$  (d) (red lines). The scale bars represent 20  $\mu\text{m}$ . [26]

The first indication that the generated beams belong to the Bessel-like beam [26] category is the transverse intensity profiles of the beams. The comparison of the transverse intensity profiles of the beams with the theoretical Bessel beam transverse intensity distribution calculated by using Eq. (1) is shown in Fig. 5. Black lines in Fig. 5(b) and Fig. 5(d) show the transverse intensity profiles of the beams, generated by different types of structures (Fig. 5(a,b) – I type, Fig. 5(c,d) – II type) at the distance of 200 μm (Fig. 5(a)) and 350 μm (Fig. 5(c)) from the sample, and red lines is the theoretical Bessel beam transverse intensity distribution calculated by using Eq. (1) when the perpendicular wave vector ( $k_{\perp}$ ) is 1.15 (Fig. 5(b)) and 0.65 (Fig. 5(d)).

The second indication that the generated beams possess the Bessel-like beam characteristics is the axial divergence of the central beam. As it is well known, the propagation of the Gaussian beam along the  $z$ -axis can be expressed by the following equation:

$$d(z) = d_0 \sqrt{1 + \left( \frac{z - z_0}{z_R} \right)^2} \quad (3)$$

where  $d_0$  is the diameter of the beam waist;  $z_0$  is the coordinate of the beam waist;  $z$  is the axial coordinate;  $z_R$  is the Rayleigh length, which can be estimated from the waist diameter and the wavelength:

$$z_R = \pi d_0^2 / (4\lambda) \quad (4)$$

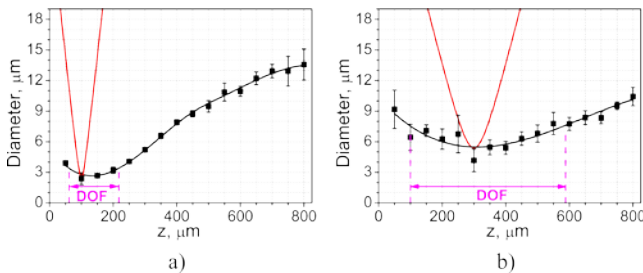


**Fig. 6** Alteration of the central spot diameter of the generated beams (black curves) by using a different type of structures: a) I type; b) II type. The black dots – the measured central spot diameter along  $z$ . The red curves show theoretically estimated divergence of the Gaussian beam when the beam waist diameter is 2.4 μm (a) and 5.4 μm (b). DOF means the depth of focus.

Comparison the divergence of the generated beam and the Gaussian beam is depicted in Fig. 6. In Fig. 6(a), the alteration of central spot diameter generated by using the I type structure is shown, and in Fig. 6(b) – using the II type structure. The divergence of the Gaussian beam (red curves) was calculated by Eq. (3). In calculations the Gaussian beam waist was adjusted to the smallest spot size of the generated beam (I type: ~ 2.4 μm; II type: ~ 5.4 μm). In this case, the calculated depth of focus of Gaussian beam is equal to ~ 17.0 μm (for I type structure) and ~ 86.1 μm (for II type structure) when the wavelength ( $\lambda$ ) is 532 nm. The depth of focus of the generated beams can be evaluated from experimental results. The depth of focus is the distance along the beam propagation direction when the beam diameter increases by  $\sqrt{2}$  comparing to its value at the

beam waist. The estimated depth of focus of the generated beams from the I and II type structures (magenta arrows in Fig. 6) is ~ 157 μm and ~ 488 μm, respectively. It is about 9 and 6 times larger than the depth of focus of the Gaussian beam. This means that the divergence of the beams generated by laser polymerised microaxicons is much lower than the divergence of the respective Gaussian beam. A negligible diffraction is one of an attribute of a Bessel-like beam.

The third feature, indicating that generated beams belong to the Bessel-like beam group, is the axial alteration of the intensity. A comparison of the axial alteration of the intensity of the generated Bessel-like beam (black curves) and Gaussian beam (red curves) with a similar initial spot size is depicted in Fig. 7. As can see from Fig. 7, the axial intensity in both cases has the modulation which is determined by the round-tip of the structures [27].

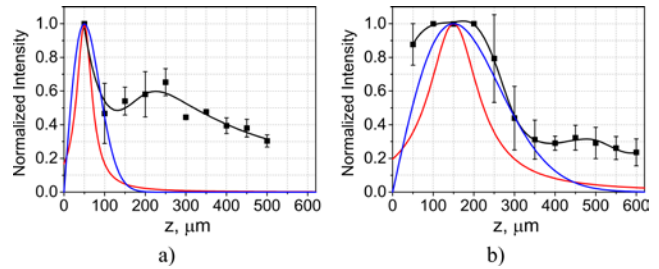


**Fig. 7** Variation of the generated beams intensity (black curves) along the axial position  $z$  from a different type of the structures: I type (a); II type (b). The black squares show the measured central spot intensity values along  $z$ . The red curves - the estimated Gaussian beam intensity distribution along  $z$  when the initial spot size is equated to the spot size at the measured highest intensity value (3.9 μm (a) and 7.1 μm (b)). The blue curves – the estimated Bessel-Gaussian beam intensity distribution lengthways  $z$  when the maximum axial intensity occurs at 50 μm (a) and 150 μm (b).

The highest intensity for I type of structure is near to the focal length distance (~ 50 μm) of the structure. For the II type structure, the highest measured intensity value is closer than the measured focal length of the structure (~ 150 μm). It can be determined by the shape of structure which is not spherical, and only the top of the structure has the spherical part (Fig. 2(b)). As can see from Fig. 7, the measured axial intensity distribution of the generated beams is declining not so fast as the Gaussian beam intensity distribution. The decrease from the maximum value of the intensity to 40% of the maximum value for the generated beams is ~ 4.5 (I type) and ~ 1.3 (II type) times lower than for the respective Gaussian beams, and this is one more proof that the generated beams possess the Bessel-like characteristics. Furthermore, the measured axial intensity distribution beyond the fabricated structures resembles the axial intensity distribution of the Bessel-Gaussian beam (blue curves in Fig. 7), which is usually obtained when the Gaussian beam passes the axicon [28]. The axial intensity of the Bessel-Gaussian beam profile is exponentially proportional to the square of the ratio of the longitudinal position and position at which maximum axial intensity occurs:

$$I(z) \sim z \exp\left(-\frac{z^2}{2z_{\max}^2}\right) \quad (5)$$

where  $z$  is the longitudinal position and  $z_{\max}=d_0/\tan\beta$  is the position at which maximum axial intensity ensues.

The Bessel-like beam arrays generated by the laser polymerised periodic structures were validated as a material treatment tool. The principle scheme of their use in laser photopolymerisation or ablation is shown in Fig. 8.

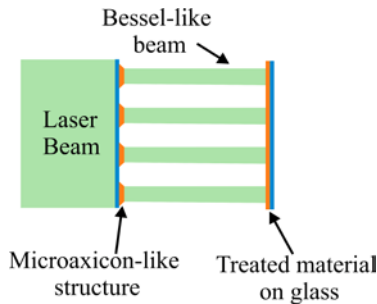


**Fig. 8** The principle utilization scheme of microaxicon-like structures in the material treatment.

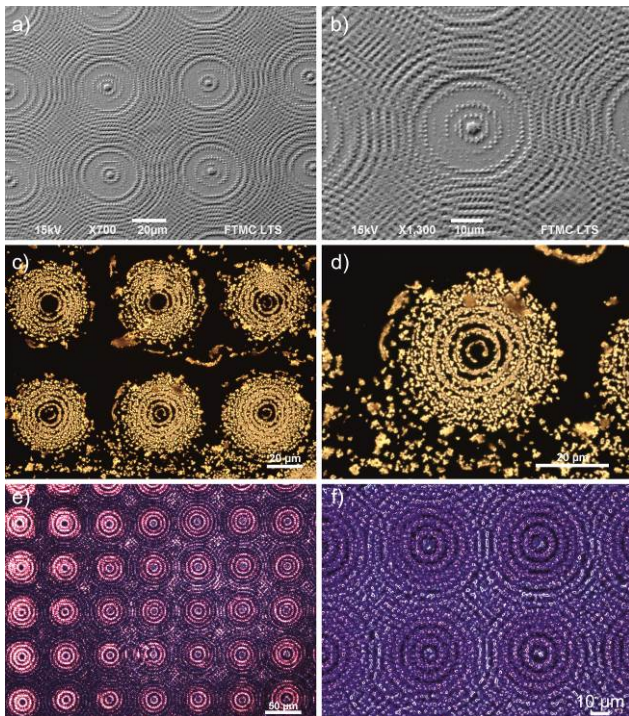


**Fig. 9** Structures fabricated by using microaxicon-like structures as the beam-forming element: a-b) SEM images of structures polymerised in SZ2080 (thickness  $\sim 10 \mu\text{m}$ ) tilted by 30 deg; c-d) optical microscope images of structures ablated in the thin gold film ( $\sim 20 \text{nm}$ ); e-f) optical microscope images of modified surface of the thin-film ink coated glass.

Periodically arranged Bessel-like beams were directed to a material process. The structures were fabricated using the method shown in Fig. 8, and are presented in Fig. 9. Different kind of structures were fabricated using the laser photopolymerisation (Fig. 9 a,b) or ablation (Fig. 9 c-f). All structures were manufactured using the I-type microaxicon-like structures as beam-forming elements. The polymerised structures (Fig. 9 a,b) were fabricated in the SZ2080 material by using  $\sim 0.81 \text{ GW/cm}^2$  peak pulse intensity and 30 s exposure time. The gold structures were manufactured with  $\sim 14 \text{ GW/cm}^2$  peak pulse intensity and 3 s exposure time. The thin-film ink coated glass surface was modified with  $\sim 19 \text{ MW/cm}^2$  peak pulse intensity and 3 s exposure time.

The fabricated structures (Fig. 9) repeat the transverse intensity distribution of Bessel beam. The diameter of the central spot of the polymerised structures is about  $3.2 \mu\text{m}$ , and it fits the central spot diameter of the used Bessel-like beam at the distance  $200 \mu\text{m}$ . The central hole of the gold structure is larger ( $\sim 4 \mu\text{m}$ ) as in this case was used the higher intensity. The central hole of some gold structures is larger twice ( $\sim 10 \mu\text{m}$ ). This is the result of the structures inhomogeneity.

After the laser treatment process, the microaxicon-like structures (Fig. 2a) were tested again by SEM in order to check if their shape remains unchanged. The test results show that the shape of microaxicon-like structures used as beam forming elements remains the same. It demonstrates that thermal stability and damage threshold of microaxicon-like structures are high, and they can be applied in beam-shaping for laser microfabrication.

The fabricated gold structures (Fig. 9c,d) can be used as metamaterials for terahertz applications as the dimensions and the periodicity of the structures perfectly fit to this range of the electromagnetic waves. The development of electromagnetic, artificial-lattice structured materials (metamaterials) can lead to the realization of phenomena that cannot be obtained with natural materials. This is necessary in the creation of THz devices which enable the construction of useful applied technologies operating within this range. The polymerised structures (Fig. 9a,b) can also be employed as templates for fabrication of thicker metallic structures by using photolithography. The created microaxicon-like structures (Fig. 2) demonstrate only a few opportunities of the generated Bessel-like beams, but they can also be used for microholes drilling or for a simple creation of angular-tolerant wavefront detectors, optical imaging systems, optical tweezers, etc.

#### 4. Conclusions

A novel and flexible strategy to create an array of the Bessel-like beams using the four-beam laser interference technique is presented. The generated beams show all fundamental features of a Bessel-like beams: 1) the transverse intensity profile matches to the Bessel beam transverse intensity distribution; 2) the axial divergence of the central spot is significantly lower comparing with that of the Gaussian beam with the same initial waist size; 3) the decline of the intensity behind the focus is either lower in comparison to the respective Gaussian beam. This result can be caused by significant spherical aberrations of the used structures. The generation of Bessel-like beams array using polymeric structures fabricated by the simple, productive and reproducible four-beam laser interference lithography technique paves the way for the creation of a novel materials treatment tool.

Validation of the optical performance of the Bessel-like beams was performed utilising the polymerised structures as a beam-shaping element in laser microprocessing. Different kind of structures was fabricated in thin gold film, in SZ2080 photopolymer and on ink-coated glass. All fabricated structures repeat the transverse intensity distribution of Bessel beam. The dimensions of the fabricated structures depends on the distance between beam-shaping element and treated sample. The dimensions and the periodicity of the manufactured structures perfectly fit to the range of

terahertz waves. Therefore, the proposed method can be useful in the fabrication of terahertz metamaterials.

### Acknowledgments

Dr Evaldas Stankevičius thanks INFOBALT Association for the nomination of personal scholarship to conduct this research.

### References

- [1] J. Durnin, J. J. Miceli, and J. H. Eberly: *Phys. Rev. Lett.* 58, (1987) 1499.
- [2] Z. Bouchal, J. Wagner, and M. Chlup: *Opt. Commun.* 151, (1998) 207.
- [3] V. Garcés-Chavez, D. McGloin, H. Melville, W. Sibbett, and K. Dholakia: *Nature* 419, (2002) 145.
- [4] T. Grosjean, D. Courjon, and C. Bainier: *Opt. Lett.* 32, (2007) 976.
- [5] X. Tsampoula, V. Garcés-Chávez, M. Comrie, D. J. Stevenson, B. Agate, C. T. A. Brown, F. Gunn-Moore, and K. Dholakia: *Appl. Phys. Lett.* 91, (2007) 053902.
- [6] J. Arlt, V. Garcés-Chavez, W. Sibbett, and K. Dholakia: *Opt. Commun.* 197, (2001) 239.
- [7] K. Dholakia and T. Cizmar: *Nat Photonics* 5, (2011) 335.
- [8] C. J. R. Sheppard and A. Choudhury: *Appl. Opt.* 43, (2004) 4322.
- [9] S. Klewitz, S. Sogomonian, P. Leiderer, and S. Herminghaus: *Opt. Lett.* 21, (1996) 248.
- [10] F. Courvoisier, J. Zhang, M. K. Bhuyan, M. Jacquot, and J. M. Dudley: *Appl. Phys. A* 112, (2013) 29.
- [11] Y. Matsuoka, Y. Kizuka, and T. Inoue: *Appl. Phys. A* 84, (2006) 423.
- [12] S. Schmid, G. Thalhammer, K. Winkler, F. Lang, and J. H. Denschlag: *New J. Phys.* 8, (2006) 159.
- [13] J. A. Kim, K. I. Lee, H. R. Noh, W. Jhe, and M. Ohtsu: *Opt. Lett.* 22, (1997) 117.
- [14] J. Arlt and K. Dholakia: *Opt. Commun.* 177, (2000) 297.
- [15] J. H. McLeod: *J. Opt. Soc. Am.* 44, (1954) 592.
- [16] A. J. Das and K. S. Narayan: *Opt. Lett.* 34, (2009) 3391.
- [17] A. Žukauskas, M. Malinauskas, C. Reinhardt, B. N. Chichkov, and R. Gadonas: *Appl. Opt.* 51, (2012) 4995.
- [18] W. C. Cheong, B. P. S. Ahluwalia, X.-C. Yuan, L.-S. Zhang, H. Wang, H. B. Niu, and X. Peng: *Appl. Phys. Lett.* 87, (2005) 024104.
- [19] R. Grunwald, S. Woggon, R. Ehlert, and W. Reinecke: *J. Eur. Opt. Soc. Part A* 6, (1997) 663.
- [20] R. Grunwald, U. Neumann, V. Kebbel, H. J. Kühn, K. Mann, U. Leinhos, H. Mischke, and D. Wulff-Molder: *Opt. Lett.* 29, (2004) 977.
- [21] E. Stankevičius, M. Malinauskas, M. Gedvilas, B. Voisiat, and G. Raciukaitis: *Mat. Sci. (Medžiagotyra)* 17, (2011) 244.
- [22] A. Ovsianikov, J. Viertl, B. Chichkov, M. Oubaha, B. MacCraith, I. Sakellari, A. Giakoumaki, D. Gray, M. Vamvakaki, M. Farsari, and C. Fotakis: *ACS Nano* 2, (2008) 2257.
- [23] E. Stankevičius, M. Malinauskas, and G. Raciukaitis: *Physics Procedia* 12, (2011) 82.
- [24] E. Stankevičius, M. Gedvilas, and G. Raciukaitis: *Appl. Phys. B* 119, (2015) 525.
- [25] R. Grunwald: "Thin Film Micro-Optics", (Elsevier, Amsterdam, 2007) p.141.
- [26] E. Stankevičius, M. Garliauskas, M. Gedvilas, and G. Raciukaitis: *Opt. Express* 23, (2015) 28557.
- [27] O. Brzobohatý, T. Cizmar, and P. Zemánek: *Opt. Express* 16, (2008) 12688.
- [28] G. Roy and R. Tremblay: *Opt. Commun.* 34, (1980) 1.

(Received: May 24, 2016, Accepted: September 15, 2016)